Facile synthesis of NiCo2O4 nanostructures with abundant surface oxygen vacancies, and reduced content of Co and Ni valence states for the efficient and bifunctional electrochemical and photocatalytic oxidation of methylene blue

Abdul Ghaffar Solangi, Aneela Tahira, Muhammad Ali Bhatti, Ahmed Ali Hulio, Abdul Sattar Chang, Zulifqar Ali Solangi, Ayman Nafady, Kangle Lv, B. Vigolo, Zafar Hussain Ibupoto

Facile synthesis of $NiCo_2O_4$ nanostructures with abundant surface oxygen vacancies, and morphological transformation using bitter gourd extract towards efficient electrocatalytic oxidation of methylene blue

Abdul Ghaffar Solangi, Aneela Tahira, Abdul Sattar Chang, Ayman Nafady, Elmuez A. Dawi, Kangle Lv, Brigitte Vigolo, and Zafar Hussain Ibupoto

1 Institute of Chemistry, Shah Abdul Latif University Khairpur Mirs, Sindh, Pakistan

2 Dr. M.A Kazi Institute of Chemistry, University of Sindh, Jamshoro 76080, Pakistan

3 Nonlinear Dynamics Research Centre (NDRC), Ajman University, P.O. Box 346, Ajman, United Arab Emirates

4 Department of Chemistry, College of Science, King Saud University, Riyadh 11451, Saudi Arabia

5 Université de Lorraine, CNRS, IJL, 54000 Nancy,France

6 College of Resource and Environment, South-Central Minzu University, Wuhan 430074, China Centre of Environmental Sciences, University of Sindh Jamshoro, Jamshoro 76080, Sindh, Pakistan

*Corresponding author(s): Zafar Hussain Ibupoto, PhD

Email : zaffar.ibhupoto@usindh.edu.pk

Abstract

An abundant, low cost, scale up and ecofriendly method has been designed about the preparation of $NiCo_2O_4$ nanostructures and as prepared electrode material was employed for the electrochemical oxidation and photocatalytic degradation of methylene blue (MB) under the irradiation of natural sunlight. The $NiCo_2O_4$ nanostructures prepared with and without spoiled bitter gourd juice were characterized with respect to morphology, crystalline quality, and surface chemical composition using different structural analysis. It was found that the morphology of $NiCo_2O_4$ nanostructures was transformed from nanorod to low dimension nanoparticles. The surface of $NiCo_2O_4$ nanostructures prepared with 10 mL of bitter gourd juice was enriched with

the abundant surface oxygen vacancies and low content of different Co and Ni valence states. The $NiCo_2O_4$ nanostructures obtained with the 10 mL of bitter gourd were highly electroactive towards the oxidation of MB in phosphate buffer solution of pH 7.4. The working range for the electrochemical oxidation of MB was estimated from 0.1mM to 7 mM and low limit of detection of 0.003mM. The 10 mL bitter gourd mediated $NiCo_2O_4$ nanostructures were highly selective, stable and reproducibility. Moreover, the $NiCo_2O_4$ nanostructures synthesized with the use of 10 mL of bitter gourd extract were also active to degrade the MB in aqueous solution under the illumination of natural sunlight. The percent removal of MB was found almost 100% for the time period of 210 min.

Kewords: $NiCo_2O_4$ nanostructures, bitter gourd juice, electrocatalytic performance, photocatalytic activity

Introduction

Methylene blue (MB) has been utilized in diverse industrial applications [1] . Methylene blue is a low molecular weight hydrophilic and cationic phenothiazinium-based dye [1]. Moreover, MB has been employed as a colorimetric probe for the detection of hydrazine and nitrite utilizing palladium nanoparticles (NPs) as a catalyst [2]. As a possible mediator and signaling probe, it has also been applied to the electrochemical detection of numerous analytes [3-6]. MB has also been used for the dying wood, silk, and cotton [7]. Despite all these potential applications of MB, it has also shown severe and harmful impacts on human health and a negative influence on the environment. The exposure of MB dye causes several diseases such as cyanosis, eye discomfort, vomiting, nausea, and respiratory problems in both humans and aquatic species [8]. Because of the presence of MB into water, it causes more dyestuffs enter water bodies, the biological oxygen demand has been raised gradually [9]. The improper dumping of MB into waterways by the food and textile industries has been realized around the world [10, 11]. From color point of view, MB has been identified one of the main component of dyes and it has been distinguished by their distinctive dark green color and bronze shine. In alcoholic and aqueous environments, MB has a rich blue color [12]. Other properties of MB including no smell and is highly stable in the atmosphere [13-17] . The initial use of MB was to identify sentinel nodes in a variety of cancers, including breast cancer [15]. Although MB is widely used in the medical profession, therefore it has several negative health consequences such as vomiting, headaches,

dizziness, hypertension, mental disorientation, excessive perspiration, abdominal pain, nausea, and precordial pain [16-19] Degrading MB into less hazardous molecules or removing it from the wastewater is highly essential and desired. Previously, MB dye can be removed either by reduction or degradation using nanomaterials including $K_2W_4O_{13}$ nanowires, graphene nanosheets, Fe_3O_4 NPs, CdS nanostructures, hematite nanoplates, and $AgFe_2O_4$/multi-walled carbon nanotubes [20-25]. On other hand, the electrocatalytic oxidation method is highly potential and alternative technology for the wastewater application. Due to facile feasibility, normal reaction conditions, zero secondary hazardous product, 100% degradation efficiency, therefore the electrocatalytic degradation methodology shows the unique and new roadmap for the practical aspect for the wastewater application [26]. The degradation process based on the electrocatalytic oxidation is mainly governed by the nature of electrode material. Highly reactive radicals generated from the anode material are in complete interaction with the organic species which are gradually degraded and oxidized, consequently transformed into mineral products [27, 28]. Recently, numerous research activities based on electrocatalytic oxidations have been performed and it has been observed that the oxidation activity has been dependent on the nature, properties, and morphology of anode material [29]. Several transition metal oxides have been noticed with high electrocatalytic performance and they are cost effective, exhibiting excellent redox effectiveness with mixed oxidation states, ecofriendly and environment friendliness [30]. For this reason, different transition metal oxides as anode materials such as Cu_2O [31], ZnO [32], Fe_2O_3 [33], PbO_2 [34], TiO_2 [35] and ATO (Sb-doped SnO_2) [36], have been employed for the wastewater application. Ternary metal oxides have superior electrocatalytic activity over binary metal oxides due to their high probability of redox pairs, spinel structure and catalytic activity [37-40]. Among the ternary metal oxides, $NiCo_2O_4$ is a mixed transition metal oxide that has excellent application in different fields such as optoelectronic devices, lithium ion batteries, super capacitors, and electrocatalysts [41-45]. As $NiCo_2O_4$ transition metal oxide is inexpensive, has a higher specific surface area, and has better electrical conductivity than the others, it has distinct qualities and nice electrochemistry. Up until this point, more $NiCo_2O_4$ nanostructures had been constructed, including $NiCo_2O_4$ @ graphene [46], Fe_2O_3 @ $NiCo_2O_4$ [47], Mno_2/ $NiCo_2O_4$ [48] and Co_2O_3/ $NiCo_2O_4$ [49, 50], which speed up the transport of electrons between the target and electrode. Nonetheless, many morphologies of $NiCo_2O_4$ have been found, including nanosheets [51], nano tubes [49] and nano sphere [47]. The

fact that so few studies have been conducted on the utilization of biomass waste to improve the electrochemical activity of $NiCo_2O_4$ through variations in shape, charge shifting, and surface defect should be more apparent. In view of the aforementioned information, good phytochemistry of bitter gourd extract biowaste has been reported for the first time to affect the shape of $NiCo_2O_4$, which exhibits the oxidation of MB. The phytochemistry of bitter gourd extract possess vicine, cryptoxanthin, neokuguaglucoside, gentisic acid, D-galacturonic acid, stearic acid, palmitic acid, stigmasterol, momordicin, charantin and oleanane [52-54].

However in this research, we show the role of bitter gourd extract, which is rich in numerous phytochemical components for modifying the surface properties of $NiCo_2O_4$ nanostructures. Using the hydrothermal technique, different amounts of bitter gourd extract were employed to modulate the surface properties of $NiCo_2O_4$.The $NiCo_2O_4$ nanostructures were found reduced in the dimension and abundant surface oxygen vacancies were produced using bitter gourd extract. These surface modifications were fully utilized towards the enhanced electrocatalytic oxidation of MB. Also, the photodegradtion of MB was also investigated using these newly synthesized $NiCo_2O_4$ nanostructures under the illumination of natural sunlight.

2. Materials and Methods

Used chemical reagents

Methylene blue, uric acid, glucose, urea, ascorbic acid, sodium chloride, potassium chloride, calcium chloride, sodium hydroxide, hydrochloric acid, disodium phosphate, and monopotassium phosphate. . All the chemicals were purchased from Sigma Aldrich Karachi, Sindh, Pakistan, and utilized without further purification.

Preparation of $NiCo_2O_4$ nanostructures using bitter gourd extract by hydrothermal method

The main precursor like A0.015M nickel chloride, 0.1M cobalt chloride, and 0.1M urea were added to 100 mL of deionized water for the efficient growth of $NiCo_2O_4$ nanostructures. The use of 0.1M urea was as a source of hydroxide ions. For preparation bench of samples, four beakers with a volume 250 mL were taken and cleaned, followed by drying at room temperature. The spoiled bitter gourd was purchased from local market located at Jamshoro and chopped into small pieces using juicer machine.

The $NiCo_2O_4$ nanostructures were prepared with the use of 5, 10, and 15 mL bitter gourd juice in three respective beakers containing 0.1M cobalt chloride, 0.015M nickel chloride and 0.1M urea by maintaining the total volume of 100 mL for each growing sample. Fourth beaker was only containing the nickel chloride, cobalt chloride and ueea with same concentration in 100 mL of deionized water and this was labeled as reference pure sample of $NiCo_2O_4$ nanostructures. All the beakers with the growth solutions were mechanically stirred for making uniform solution and covered with aluminum foil and kept in an electric oven at a temperature of 95 °C for 5 hours. After that, ordinary laboratory filter paper was used to obtain hydroxide phase of nickel and cobalt and washed several times with the deionized water and ethanol, finally left to dry for overnight at 60 ^oC. Later, the dried samples of nickel-cobalt hydroxide phase were thermally brunt at 500 ^oC for 5 hours in muffle furnace and air.

Material Characterization

The crystalline structure of $NiCo_2O_4$ nanostructures was studied using powdered X- ray diffraction with CuKα radiation ($1.548A^0$) and applying potential of 45 kV and applying current of 45 mA. While morphology of $NiCo_2O_4$ nanostructures was investigated using scanning electron microscopy (SEM) at 10 kV.

Electrochemical investigations onto $NiCo_2O_4$ nanostructures

To evaluate the electrocatalytic properties of $NiCo_2O_4$ nanostructures for the oxidation of MB, different electrochemical modes such as cyclic voltammetry (CV), linear scanning voltammetry (LSV), chronoamperometry (CA) and electrochemical impedance spectroscopy (EIS) were used. The 10 mg of $NiCo_2O_4$ nanomaterial was dispersed in 2.5 mL of deionized water water, adding 0.5 mL of Nafion (5%) and using a sonicator to obtain a uniform suspension. Glassy carbon electrode (GCE, 3mm) washed with the deionized water after being cleaned with an alumina paste. $NiCo_2O_4$ nanomaterial was dropped onto GCE using the drop casting technique. Bare glassy carbon electrode (BGC) and modified (MGCE) were employed to investigate the electrochemical oxidation of MB. In a three-electrode system, GCE was utilized as the working electrode, Pt wire served as the counter electrode, and silver-silver chloride (Ag/AgCl, 3.0M KCl) was employed as the reference electrode. A 0.lM phosphate buffer solution of pH 7.4 was

used to prepare 50 mM MB stock solution. For each electrochemical test, PBS was used as a supporting electrolyte. The selectivity of electrocatalytic properties of $NiCo_2O_4$ nanostructures was monitored in the presence of , ascorbic acid, uric acid, sodium ions, chloride ions, potassium ions, calcium ions, and other interfering having concentration of 0.1mM solution in the deionized water. The limit of detection was estimated using the reported work as reference [55]. The photocatalytic aspects of pure $NiCo_2O_4$ nanostructures and bitter gourd juice mediated samples were studied against Photodegradation of MB under the illumination of natural sunlight. The measurements were done according to reported work [56]. The suspension of 5 mg photocatalyst and 2.3×10^{-6} M MB dye was stirred in the dark for 30 min to achieve adsorption/desorption equilibrium between the MB molecules and the photocatalyst prior to natural sunlight exposure. All the photocatalytic experiments were then in the month of May 2023 in between 12 pm to 2.30 pm. Using double beam UV-visible spectrophotometer, the absorbance of the MB solution associated with photocatalyst in the wavelength range 400-800 nm was measured for every 35 minutes to determine the photocatalytic degradation [57].

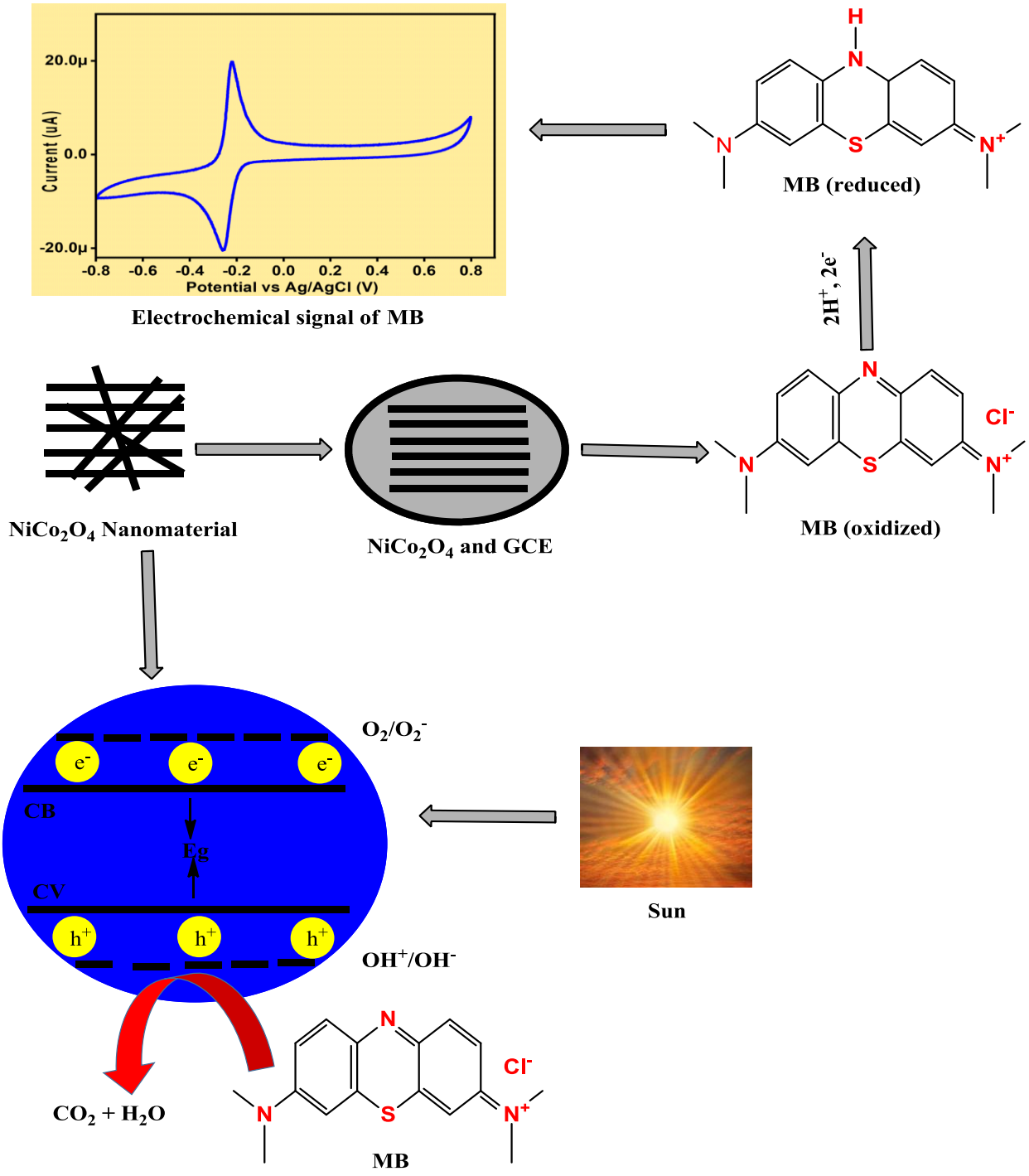

Scheme 1: Stepwise oxidation of MB and photo catalytic activity by $NiCo_2O_4$ using bitter gourd extract

3. Results and Discussion:

$NiCo_2O_4$ nanostructures were prepared using different amounts of bitter gourd extract (5, 10 and 15 mL), and their crystalline structure was examined by powered XRD. The diffraction patterns of all the prepared $NiCo_2O_4$ nanostructures are depicted in Figure 1. Various XRD peaks for as prepared $NiCo_2O_4$ nanostructures were located at 19.40, 31.30, 36.88^o, 38.59^o, 44.85^o, 59.41^o, and 65.30^o, and corresponding crystallographic planes (111), (220), (311), (222), (400), (511) and (440) were noticed. The XRD patterns were fully agreed with the JCPDS 01-073-1702. The use of bitter gourd juice was enhanced and peak intensity of $NiCo_2O_4$ nanostructures, suggesting the improved crystal quality. Also, it has been noted that the bitter gourd juice carried variety of macromolecules and phytochemicals which strongly influence on the surface properties of $NiCo_2O_4$. With the addition of various amounts of bitter gourd juice, SEM images were collected for the verification of shape orientation of $NiCo_2O_4$ nanostructures as shown in Figure 2.. Figures 2a describes the rod like morphology of $NiCo_2O_4$ nanostructures without the use of bitter gourd juice. The size of nanorods of $NiCo_2O_4$ could be few microns in length and an average diameter of 300-500 nm.. When comparing different SEM pictures of $NiCo_2O_4$ grown with varying amounts 5 mL, 10 mL and 15 mL of bitter gourd extract as shown in Figure 2b-d The preparation of $NiCo_2O_4$ nanostructures with addition of bitter gourd juice has changed the rod like structure into nanoparticles and size each $NiCo_2O_4$ nanostructures was below 200 nm. . Due to the presence of specific phytochemicals from bitter gourd juice during the growth phase, they play a crucial role in decreasing the size of $NiCo_2O_4$ nanostructure from micron to nm. This is highly increased the surface via reduction in the dimension of $NiCo_2O_4$ nanostructures prepared with the use of bitter gourd juice. Hence, this can further be highly desirable for the improving the electrochemical oxidation of MB.

HRTEM was used to examine other morphological features in greater detail, as shown in Fig. 1. As seen in Fig. 1(a), pure material exhibits spherical irregular forms all around [58, 59]. These lattice fringes values, however, were estimated using Image-J softwar [60, 61] . The related d-spacing value from lattice fringes has been estimated as 0.40 nm, as well as the Fast Fourier Transform (FFT) pattern of lattice fringes, which can be seen on the right side of the

accompanying image. Furthermore, the elemental mapping of as-prepared material is shown in Fig. 1. (b, c, d, and e). Additionally, the targeted material's lattice fringes have been computed as 0.48 nm, together with its FFT transformation on the right side of the relevant picture, depicted in Fig. 2 (a) [62, 63]. The existence of desirable elements such as Co, Ni, and O has been established by elemental mapping and EDS. Fig. 2 (b, c, d, and e) depicts the elemental mapping of produced material, and EDS spectra respectively.

The XPS analysis was performed onto $NiCo_2O_4$ nanostructures prepared with 10mL of bitter gourd juice to evaluate the valence states of nickel and cobalt and surface oxygen vacancies as shown in Figure 5. While the XPS results of pure $NiCo_2O_4$ nanostructure were described in our previous work [64]. because preparation conditions were similar for pure $NiCo_2O_4$ nanostructures reported in this work. The typical Co(III) and Co(II) peaks were noticed in the highly two spin resolved spectrum at 779.46 eV and 780.55 eV respectively, while two satelllite peaks were also found at 785.00 eV and 789.10 eV as shown in Figure 5a. The relative % of Co(III) and Co(II) were observed as 17.56 % and 69.09%, suggesign the low abundance of these cobalt oxidation states comapred to pure $NiCo_2O_4$ nanostructure reported by our group [64]. . Similarly, highly resolved spectrum was also measured using Voigt fitting model as shown in Figure 5b. The Ni 2p spectrum was dominated by the presence of Ni(II) and (NIII) oxidation states characterized through spin orbit doublet peaks at 853.88 eV and 855.62 eV respectively [48, 65]. The comparison of these oxidation of states of Ni was also carried out though the estimation of relative percentage such as for Ni(II) and Ni(III) as 5.82 % and 59.10% respectively. Also, a satellite peak was noticed in the Ni 2p spectrum at 861.27 eV as shown in Figure 5b. The O 1s spectrum of $NiCo_2O_4$ nanostructures synthesized with 10 mL of bitter gourd juice was also recorded for the illustration of metal-oxygen bonds in order to verify the formation of bimetallic oxides of $NiCo_2O_4$ nanostructures and fitted spectrum is shown in Figure 5c. There are three distinctive peaks noticed in the fitted O 1s spectrum of $NiCo_2O_4$ nanostructures located at 529.61 eV, 531.07 eV, and 532.95 eV attributed to typical metal-oxygen bond, oxygenated ions (O^-) and chemi/phsyico adsorbed species onto $NiCo_2O_4$ nanostructures as described in the previous results published by our group [64]. The relative percentage of metal-oxygen bonds, oxygenated ions and surface adsorbed species was 42.15%, 49.14%, and 8.71% respectively, suggesting the lower amount of $NiCo_2O_4$ nanostructures due to surface reduction caused by the bitter gourd phytochemicals compared to the pure $NiCo_2O_4$

nanostructures as reported previously. Overall XPS analysis has revealed that the surface of $NiCo_2O_4$ nanostructures was enriched with the low concentration of Co, and Ni ions and abundant surface oxygen vacancies, and such aspects at the surface of nanomaterial are highly favorable for the efficient electrocatalytic applications [48].

3.2 Electrochemical oxidation of methylene blue on $NiCo_2O_4$ nanostructures prepared with bitter gourd juice

The role of different amounts of bitter gourd juice on the electrochemical performance of $NiCo_2O_4$ nanostructures was investigated during the oxidation of methylene blue in phosphate buffer solution (PBS) of pH 7.4. The preliminary electrochemical analysis was carried out using cyclic voltammetry (CV) at a scan rate of 50 mV/s. The electrochemical activity of various $NiCo_2O_4$ nanostructures prepared with 5, 10 and 15 mL of bitter gourd juice and pure $NiCo_2O_4$ nanostructures was tested using CV at a scan rate of 5 mV/s in 0.5mM MB prepared in 0.1M PBS of pH 7.4 as shown in Figure 6a. It could be seen that there is large variability in the electrochemical performance of $NiCo_2O_4$ nanostructures preared with and without bitter gourd, indicating the major contribution of phytochemicals from bitter gourd for enhancing the electrocatalytic activity as prepared nanomaterial. Likewise, the CV curves of 10 mL bitter gourd induced $NiCo_2O_4$ nanostructures in 0.5mM MB and in 0.1M PBS solution of pH 7.4 were compared with the bare glassy carbon electrode under same analyte and electrolyte conditions as shown in Figure 6b. It was observed clearly that $NiCo_2O_4$ nanostructures prparedd with 10 mL of bitter gourd juice has shown excellent electrocatalytic performance in the presence of 0.5 mM MB, however the electrochemical performance of $NiCo_2O_4$ nanostructures prepared with 10 mL bitter gourd juice in PBS of pH of 7.4 was seen negligible and similar trend was also observed for the bare glassy carbon electrode (BGCE) as shown in Figure 6b. The CV analysis has revealed that the electrocatalytic activity of $NiCo_2O_4$ nanostructures was significantly improved when 10 mL of bitter gourd was used. It has been previously reported that the electrocatalytic performance of nanomaterial is highly dependent on the size, shape, enriched surface with abundant catalytic sites, and defects in the structure. These factors were highly dominant in the morphological transformation, surface defects in terms of oxygen vacancies, reduced content of Co and Ni valence states, and the size of $NiCo_2O_4$ nanostructures during the use of 10 mL of bitter gourd juice and these aspects were observed by using various analytical techniques such as

XRDM SEM, TEM and XPS. General oxidation process of MB onto $NiCo_2O_4$ nanostructures could be illustrated through CV results. It was observed that the oxidation of MB has shown the provision of electrons which were taken by the $NiCo_2O_4$ nanostructures as could be seen from the increased oxidation peak current while the reduction peak was relatively asscoaietd with low peak current. The use of $NiCo_2O_4$ nanostructures towards oxidation of MB and the possible reaction mechanism would be described according to the developed non-enzymatic sensor configurations based on $NiCo_2O_4$ nanostructures [66, 67].

$$NiCo_2O_4 + OH^- + H_2O \longrightarrow NiOOH + 2CoOOH + e^- \quad (5)$$

$$CoOOH + OH^- \longrightarrow CoO_2 + H_2O + e^- \quad (6)$$

$$Ni\ (II) + Co\ (II) \longrightarrow Ni\ (III) + Co\ (III) + 2e^- \quad (7)$$

The oxidation of MB onto $NiCo_2O_4$ nanostructures might reduce the Co^{3+} and Ni^{3+} to Co^{2+} and Ni^{2+} ionic species. From the structural information point fo view, the reduced particle size, shape transformation, increased surface oxygen vacancies and enriched surface active sites could favored the generation of strong electrical signal during the oxidation of MB onto $NiCo_2O_4$ nanostructures. Moreover, the electrode kinetics of modified electrode with the $NiCo_2O_4$ nanostructures prepared with 10 mL of bitter gourd juice was investigated through CV study at different scan rates ranging from 10 mV/s to 190 mV/s in 0.5mM MB as shown in Figure 7a. It could be noticed that every CV curve was characterized with oxidation and reduction peaks, suggesting the reversible behavior of electrode in 0.5mM MB. Also, the electrode kinetics was found kinetically controlled due to the successive rise of oxidation and reduction peak current with the increasing scan rate as shown in Figure 7a. It was noticed that there was a linear correlation between the increasing scan rates increasing oxidation peak current as shown in Figure 7b. A regression coefficient value of (R^2 = 0.99) has confirmed the high accuracy and precision of electrode material for the oxidation of MB towards the development of analytical method. These aspects of electrode performance were demonstrating the controlled surface adsorption and electrochemical activity. Interestingly, it was also observed during the scan rate study, there was slight shift in th oxidation peak potential, indicating the slow electron transfer during the oxidation of MB as scan rate was successively increased.

Electrocatalytic activity of $NiCo_2O_4$ nanostructures prepared with 10 mL of bitter gourd juice towards oxidation of MB

It is an important phenomenon to identify the working range of $NiCo_2O_4$ nanostructures towards the oxidation of MB in PBS of pH 7.4, thus the CV polarization curves at 50 mV/s were recorded with increasing concentrations of MB as shown in Figure 8a. It was evidently found that there is a direct correlation between the concentration of MB and the oxidation peak current, consequently oxidation peak current was found higher in the high concentration of MB. For this purpose, different concentrations MB were prepared in 0.1M PBS of pH 7.4 and 10 mL of bitter gourd juice mediated $NiCo_2O_4$ nanostructures were employed as an electrode material to identify the working range towards oxidation of MB as shown in Figure 8a. The linear relationship between MB concentration and oxidation current was build and fitted data is shown in Figure 8b. The linear fitting revealed an outstanding analytical aspect of 10 mL mediated $NiCo_2O_4$ nanostructures towards the oxidation of MB with regression coefficient ($R^2 = 0.99$) and working range for the oxidation of MB was in the range between 0.1 mM to 7.0 mM as shown in Figure 8b. The point of care was noticed during the electrochemical measurements on $NiCo_2O_4$ nanostructures for the verification of working range, the material has shown limitation to show strong signal below 0.1mM and above 7 mM because of the limitations and saturation aspects respectively. The limit of defection (LOD) and limit of quantification (LOQ) were also estimated using previously reported method [55]. The estimated LOD was around 0.002 mM and LOQ about 0.008 mM. A high working linear range, and low LOD values compared the different methods developed for the oxidation of MB and other methods have been observed for the presented $NiCo_2O_4$ nanostructures. This has authenticated that proposed electrode configuration based on $NiCo_2O_4$ nanostructures could be utilized as an alternative method for the reliable and précised detection of MB from the wastewater samples. Furthermore, to validate the performance of $NiCo_2O_4$ nanostructures in terms of working range, linear sweep voltammetry (LSV) was also employed to ensure the linear range of electrode materials the oxidation of MB. The observed LSV characterization of $NiCo_2O_4$ nanostructures has been depicted in Figure 9a and the current was successively enhanced with increasing MB concentration, indicating the sensitive electrical generation. The linear plot was fitted between generated current and successive addition of MB concentration as shown in Figure 9b. Again, the well-fitting was proven through the regression coefficient ($R^2 = 0.99$) as shown in Figure 9b.The LSV study has

presented an excellent electrocatalytic activity of $NiCo_2O_4$ nanostructures prepared with 10 mL of bitter gourd juice towards oxidation of MB in PBS of pH 7.4. To evaluate the selective aspects of $NiCo_2O_4$ nanostructures prepared with 10 mL of bitter gourd juice, CV cycles were measured in the presence of different competing dyes and other ionic species such as methylene orange, phenolphthalein, sodium ion, potassium ion, calcium ion, glucose and ascorbic acid in 0.5 mM MB as shown in Figure 10a. It could be seen that the add k ion of these interfering agents did not alter the oxidation peak current and oxidation potential, confirming the high selectivity of as synthesized $NiCo_2O_4$ nanostructures. The relative variation in the peak current against the addition of each interfering was represented by bar graphs as shown in Figure 10b. It was clearly seen that the addition of each interring agent in the MB solution did not effect on the peak current and less than 3% deviation was noticed compared to the peak current of MB oxidation, suggesting that high potential of $NiCo_2O_4$ nanostructures to selectivity oxidize MB under the microenvironment of these interfering agents as shown in Figure 10b. The stability of modified electrode with $NiCo_2O_4$ nanostructures was also investigated by measuring the 20 CV curves at 5 mV/s in 0.5 mM MB and electrode has shown outstanding the stability for the confirming the mechanical and chemical durability as shown in Figure 11a. The electrode did not show any variability in the peak current and peak potential during the oxidation of Mb, verifying that it could be used for the continuous electrochemical oxidation of MB in PBS of pH 7.4. Moreover, the reproducibility of modified electrode with $NiCo_2O_4$ nanostructures was studied using 20 independent electrodes in 0.5 mM MB by CV measurement and the corresponding the variation in the peak current of each electrode has been shown in bar graph as depicted in Figure 11b. It was found that the variability in the current generation during the oxidation of MB was less than 5%, revealing the excellent electrode-electrode electrical signal. Based on the performance of $NiCo_2O_4$ nanostructures prepared with 10 mL of bitter gourd juice during the oxidation of MB in terms of linear range, selectivity, limit of detection, reproducibility and stability show the most potential electrocatalytic material for diverse applications. The performance evaluation was made for the dominant activity of $NiCo_2O_4$ nanostructures synthesized with 10 mL of bitter gourd juice with the electrochemical and other methods as given in Table 1. The proposed electrode material is outperforming oxidation of MB for the wide linear range, facile synthesis, scale up material production, easy to operate, low cost and ecofriendly compared to many recently reported methods. In addition to electrochemical

oxidation performance of $NiCo_2O_4$ nanostructures prepared with different content of bitter gourd juice, the photoddegradation of MB was also studied under the irradiation of natural sunlight. Typical molar absorptivity of MB was noticed at 664 nm and the relative decrease in the absorbance of MB solution associated with photocatalysts at different irradiated times was carried out. The Figure 12 shows the Photodegradation of MB under the irradiation of natural sunlight using as prepared $NiCo_2O_4$ nanostructures with 5 mL, 10 mL of bitter gourd juice and without bitter gourd. Importantly, the degradation of MB using $NiCo_2O_4$ nanostructures with bitter gourd has shown dramatic decrease in the absorbance with time when the dye solution was exposed to natural sunlight. Also, the $NiCo_2O_4$ nanostructures prepared with 10 mL of bitter gourd juice has described highly enhanced photocatalytic performance towards MB degradation under the irradiation of natural sunlight as shown in Figure 12c. It was noticed that the dye was almost removed 100% when time of 210 min reached for the 10 mL bitter gourd mediated $NiCo_2O_4$ nanostructures as shown in Figure 12c. A significant and improved performance for the MB degradation under the illumination of natural sunlight could be attributed form the enriched surface active sites, low charge recombination rate ion electron-hole pairs and highly favorable surface of $NiCo_2O_4$ nanostructures prepared with 5 mL and 10 mL of bitter gourd juice compared to the pure $NiCo_2O_4$ nanostructures. The degradation kinetics of MB dye associated with $NiCo_2O_4$ nanostructures was also evaluated for the estimation of reaction mechanism and the rate constant. After the fitting, it was noticed that the degradation of MB using $NiCo_2O_4$ nanostructures followed pseudo first order kinetics where the degradation of MB was dominated by the dye and following equation was used to describe the dye degradation kinetics [68].

$$\ln (C_t / C_o) = - k_t \quad \ldots\ldots\ldots\ldots\ldots\ldots\ldots\ldots\ldots\ldots \quad (8)$$

Herein, C_o, and C_t stand for initiation dye concentration and the various time dependent dye concentration, while k is the rate constant. The kinetics plots have reveal that the MB degradation was highly time dependent in the presence of $NiCo_2O_4$ nanostructures and abruptly increased with the use of 10 mL of bitter gourd juice and followed the pseudo first order kinetics as shown in Figure 13. Importantly, the dye removal was estimated almost 100% for the $NiCo_2O_4$ nanostructures prepared with 10 mL of bitter gourd juice as shown in Figure 13c.

Table 1: Performance comparison of the enzyme-free sensor based on $NiCo_2O_4$ nanostructures grown with 10 mL bitter gourd extract versus several non-enzymatic MB sensors in the literature.

Method	**Technique**	**Linear range**	**Limit of detection**	**References**
Optical	Fluorometric	0 –13626 (µg/L)	131.14 (µg/L	[69]
	SERS	3-319.85 (µg/L)	3 (µg/L)	[56]
	UV-vis (spectrophotometry)	0.31–28.5 (µM)	-	[70]
	UV-vis (spectrophotometry)	0.63– 219 (µM)	0.19 (µM)	[71]
Electrochemical	DPV	1599.3–12794 (µg/L)	-	[72]
	DPV	0.01 – 1.1 (µM)	3.9 (µM)	[1]
	Potentiometry	1 – 3000 (µM)	0.765 (µM)	[73]
	CV	319.85–4478 (µg/L)	127.94 (µg/L)	[74]
	CV	1–10 (µg/L)	0.7 (µg/L)	[75]
	CV	1 – 14 (µM)	0.4 (µM)	[74]
	CV	100–7000 (µM	-	Present work

Table 2: The comparative studies of presented results with previous work

Catalyst	Weight	Light Source	Dye Concentration	Time (min)	Dye Removal (%)	Method	Ref.
TiO_2@ Bi_2O_3	35 mg	Sun light	2 mg catalyst (50 mL of dye solution)	250	94	Green synthesis	[76]
TiO_2 NPs	100 mg	UV-Irradiation	100 mL MB	120	92	Chemical and green synthesis methods	[77]

$TiOSO_4$	0.1 g	UV-Irradiation	20 ppm MO	150	94	Sol-gel method	[78]
$MnTiO_3$	5 mg	Sun light	MB $1x10^{-5}$M	250	75	Sol-gel	[79]
Fe_2TiO_5	50 mg	Sun light	MB 10 mg L^{-1}	250	97	Sol-gel	[80]
W doped ZnO	20 mg	UVlight	MB	3 h	96.9	Low temperature aqueous chemical growth method	[81]
TiO_2 Ficus carica leaves extract	2 mg	Solar light	$5x10^{-5}$M (MB)	330	98.82	Simple hydrothermal process	[82]
$NiCo_2O_4$ Bitter gourd extract	5 mg	Sun light	2.3×10^{-6}M (MB)	210 (min)	100	Simple hydrothermal process	Current work

Conclusions

In summary, $NiCo_2O_4$ nanostructures were synthesized using bitter gourd juice during the hydrothermal method and investigated against the electrochemical oxidation and photocatalytic degradation of MB. The structural characterization has revealed that the shape transformation was evidently taken place from rod to small dimension nanoparticles, abundant surface oxygen vacancies, and low content of Co and Ni valence states on the surface for the $NiCo_2O_4$ nanostructures synthesized with 10 mL of bitter gourd juice. The $NiCo_2O_4$ nanostructures obtained with 10 mL of bitter gourd juice, have shown outstanding electrocatalytic performance towards oxidation of MB phosphate buffer solution of pH 7.4. The working range for the oxidation of MB was estimated between 0.1mM and 7 mM. The LOD was approximately 0.003 mM. Also, the high stability, selectivity and reproducibility of $NiCo_2O_4$ nanostructures were found highly satisfactory. Furthermore, the $NiCo_2O_4$ nanostructures synthesized with and without bitter gourd juice were employed as a photocatalyst for the degradation of MB under the irradiation of natural sunlight. The dye removal was found almost 100% with the use of 10 mL of bitter gourd mediated $NiCo_2O_4$ nanostructures. The obtained electrochemical and photocatalytic performance of $NiCo_2O_4$ nanostructures suggest that bitter gourd could be employed for the synthesis of efficient, low cost, scale up and ecofriendly nanomaterial's for the diverse applications for instance biomedical, environmental, energy conversion and storage etc.

References

[1] B.H. Vilsinski, P.R. Souza, A.C. de Oliveira, M. César Filho, A.J. Valente, E.C. Muniz, O. Borges, A.P. Gerola, W. Caetano, A.F. Martins, Photophysics and drug delivery behavior of methylene blue into Arabic-gum based hydrogel matrices, Materials Today Communications, 26 (2021) 101889.

[2] N. Pourreza, R. Abdollahzadeh, Colorimetric determination of hydrazine and nitrite using catalytic effect of palladium nanoparticles on the reduction reaction of methylene blue, Microchemical Journal, 150 (2019) 104067.
[3] J. Chang, W. Lv, Q. Li, H. Li, F. Li, One-step synthesis of methylene blue-encapsulated zeolitic imidazolate framework for dual-signal fluorescent and homogeneous electrochemical biosensing, Analytical Chemistry, 92 (2020) 8959-8964.
[4] D. Liu, S. Meng, X. Shen, Y. Li, X. Yan, T. You, Dual-ratiometric aptasensor for streptomycin detection based on the in-situ coupling of photoelectrochemical and electrochemical assay with a bifunctional probe of methylene blue, Sensors and Actuators B: Chemical, 332 (2021) 129529.
[5] C. Wang, Q. Zhao, A reagentless electrochemical sensor for aflatoxin B1 with sensitive signal-on responses using aptamer with methylene blue label at specific internal thymine, Biosensors and Bioelectronics, 167 (2020) 112478.
[6] L.-L. Zhao, H.-Y. Pan, X.-X. Zhang, Y.-L. Zhou, Ultrasensitive detection of microRNA based on a homogeneous label-free electrochemical platform using G-triplex/methylene blue as a signal generator, Analytica chimica acta, 1116 (2020) 62-69.
[7] Z. Li, Z. Jia, T. Ni, S. Li, Adsorption of methylene blue on natural cotton based flexible carbon fiber aerogels activated by novel air-limited carbonization method, Journal of Molecular Liquids, 242 (2017) 747-756.
[8] G. Kathiresan, K. Vijayakumar, A.P. Sundarrajan, H.-S. Kim, K. Adaikalam, Photocatalytic degradation efficiency of ZnO, GO and PVA nanoadsorbents for crystal violet, methylene blue and trypan blue dyes, Optik, 238 (2021) 166671.
[9] S. Pandey, J.Y. Do, J. Kim, M. Kang, Fast and highly efficient catalytic degradation of dyes using κ-carrageenan stabilized silver nanoparticles nanocatalyst, Carbohydrate polymers, 230 (2020) 115597.
[10] S. Shakoor, A. Nasar, Adsorptive treatment of hazardous methylene blue dye from artificially contaminated water using cucumis sativus peel waste as a low-cost adsorbent, Groundwater for Sustainable Development, 5 (2017) 152-159.
[11] M.O. Pacheco-Álvarez, A. Picos, T. Pérez-Segura, J.M. Peralta-Hernández, Proposal for highly efficient electrochemical discoloration and degradation of azo dyes with parallel arrangement electrodes, Journal of Electroanalytical Chemistry, 838 (2019) 195-203.
[12] M.A. Hossain, M.M. Ali, T.S. Islam, Comparative adsorption of Methylene Blue on different low cost adsorbents by continuous column process, International Letters of Chemistry, Physics and Astronomy, 77 (2018) 26-34.
[13] K.-H. Kim, S.-K. Ihm, Heterogeneous catalytic wet air oxidation of refractory organic pollutants in industrial wastewaters: a review, Journal of Hazardous Materials, 186 (2011) 16-34.
[14] M. Hayat, A. Shah, J. Nisar, I. Shah, A. Haleem, M.N. Ashiq, A novel electrochemical sensing platform for the sensitive detection and degradation monitoring of methylene blue, Catalysts, 12 (2022) 306.
[15] P.I. Haigh, N.M. Hansen, K. Qi, A.E. Giuliano, Biopsy method and excision volume do not affect success rate of subsequent sentinel lymph node dissection in breast cancer, Annals of surgical oncology, 7 (2000) 21-27.
[16] C. Peter, D. Hongwan, A. Küpfer, B. Lauterburg, Pharmacokinetics and organ distribution of intravenous and oral methylene blue, European journal of clinical pharmacology, 56 (2000) 247-250.
[17] M. Salhab, W. Al Sarakbi, K. Mokbel, Skin and fat necrosis of the breast following methylene blue dye injection for sentinel node biopsy in a patient with breast cancer, International Seminars in Surgical Oncology, Springer, 2005, pp. 1-3.
[18] S.W. Bai, E.H. Huh, D.J. Jung, J.H. Park, K.H. Rha, S.K. Kim, K.H. Park, Urinary tract injuries during pelvic surgery: incidence rates and predisposing factors, International Urogynecology Journal, 17 (2006) 360-364.

[19] O. Lipskikh, E. Korotkova, Y.P. Khristunova, J. Barek, B. Kratochvil, Sensors for voltammetric determination of food azo dyes-A critical review, Electrochimica Acta, 260 (2018) 974-985.
[20] Q.-S. Huang, W. Wei, J. Sun, S. Mao, B.-J. Ni, Hexagonal K2W4O13 nanowires for the adsorption of methylene blue, ACS Applied Nano Materials, 2 (2019) 3802-3812.
[21] M.S. Nas, AgFe2O4/MWCNT nanoparticles as novel catalyst combined adsorption-sonocatalytic for the degradation of methylene blue under ultrasonic irradiation, Journal of Environmental Chemical Engineering, 9 (2021) 105207.
[22] A. Singh, P. Khare, S. Verma, A. Bhati, A.K. Sonker, K.M. Tripathi, S.K. Sonkar, Pollutant soot for pollutant dye degradation: soluble graphene nanosheets for visible light induced photodegradation of methylene blue, ACS Sustainable Chemistry & Engineering, 5 (2017) 8860-8869.
[23] S. Song, Y. Wang, H. Shen, J. Zhang, H. Mo, J. Xie, N. Zhou, J. Shen, Ultrasmall graphene oxide modified with Fe3O4 nanoparticles as a fenton-like agent for methylene blue degradation, ACS Applied Nano Materials, 2 (2019) 7074-7084.
[24] S. Thakur, P. Das, S.K. Mandal, Solvent-induced diversification of CdS nanostructures for photocatalytic degradation of methylene blue, ACS applied nano materials, 3 (2020) 5645-5655.
[25] M. Zong, D. Song, X. Zhang, X. Huang, X. Lu, K.M. Rosso, Facet-dependent photodegradation of methylene blue by hematite nanoplates in visible light, Environmental Science & Technology, 55 (2020) 677-688.
[26] F. Wang, Y. Mo, L. Sun, S. Wang, S. Cui, H. Wang, J. Li, Performance deterioration of Sb-SnO2/C membrane anode treating phenolic wastewater and anode regeneration: Adsorption and physicochemical change of catalysts, Separation and Purification Technology, 277 (2021) 119555.
[27] B.P. Chaplin, Critical review of electrochemical advanced oxidation processes for water treatment applications, Environmental Science: Processes & Impacts, 16 (2014) 1182-1203.
[28] C.F. Machado, M.A. Gomes, R.S. Silva, G.R. Salazar-Banda, K.I. Eguiluz, Time and calcination temperature influence on the electrocatalytic efficiency of Ti/SnO2: Sb (5%), Gd (2%) electrodes towards the electrochemical oxidation of naphthalene, Journal of Electroanalytical Chemistry, 816 (2018) 232-241.
[29] Y. Liao, Y. Gao, S. Zhu, J. Zheng, Z. Chen, C. Yin, X. Lou, D. Zhang, Facile fabrication of N-doped graphene as efficient electrocatalyst for oxygen reduction reaction, ACS Applied Materials & Interfaces, 7 (2015) 19619-19625.
[30] Q. Huo, J.G. Worden, Monofunctional gold nanoparticles: synthesis and applications, Journal of Nanoparticle Research, 9 (2007) 1013-1025.
[31] S. Mao, X. Sun, H. Qi, Z. Sun, Cu2O nanoparticles anchored on 3D bifunctional CNTs/copper foam cathode for electrocatalytic degradation of sulfamethoxazole over a broad pH range, Science of The Total Environment, 793 (2021) 148492.
[32] S. Payra, S. Challagulla, Y. Bobde, C. Chakraborty, B. Ghosh, S. Roy, Probing the photo-and electro-catalytic degradation mechanism of methylene blue dye over ZIF-derived ZnO, Journal of hazardous materials, 373 (2019) 377-388.
[33] H. Ma, Q. Zhuo, B. Wang, Electro-catalytic degradation of methylene blue wastewater assisted by Fe2O3-modified kaolin, Chemical Engineering Journal, 155 (2009) 248-253.
[34] J. Lyu, H. Han, Q. Wu, H. Ma, C. Ma, X. Dong, Y. Fu, Enhancement of the electrocatalytic oxidation of dyeing wastewater (reactive brilliant blue KN-R) over the Ce-modified Ti-PbO 2 electrode with surface hydrophobicity, Journal of Solid State Electrochemistry, 23 (2019) 847-859.
[35] X. Guo, D. Li, J. Wan, X. Yu, Preparation and electrochemical property of TiO2/Nano-graphite composite anode for electro-catalytic degradation of ceftriaxone sodium, Electrochimica Acta, 180 (2015) 957-964.

[36] H. Zhang, J. Qian, J. Zhang, J. Xu, Preparation of TiO 2@ Sn (Sb) O 2 core–shell composites and their applications for electrocatalytic degradation of methylene blue, Journal of Materials Science: Materials in Electronics, 32 (2021) 2026-2040.
[37] S. Chen, G. Yang, Y. Jia, H. Zheng, Three-dimensional NiCo 2 O 4@ NiWO 4 core–shell nanowire arrays for high performance supercapacitors, Journal of Materials Chemistry A, 5 (2017) 1028-1034.
[38] X. Wu, S. Li, B. Wang, J. Liu, M. Yu, Controllable synthesis of micro/nano-structured MnCo 2 O 4 with multiporous core–shell architectures as high-performance anode materials for lithium-ion batteries, New Journal of Chemistry, 39 (2015) 8416-8423.
[39] C.-Y. Yu, J.-S. Park, H.-G. Jung, K.-Y. Chung, D. Aurbach, Y.-K. Sun, S.-T. Myung, NaCrO 2 cathode for high-rate sodium-ion batteries, Energy & Environmental Science, 8 (2015) 2019-2026.
[40] L. Liu, C. Chen, J. Xing, Z. He, J. Xu, Facile synthesis of NiCo2O4 porous nanotubes with excellent electrocatalytic properties for methylene blue degradation, Journal of Materials Science: Materials in Electronics, 33 (2022) 7212-7226.
[41] J. Li, S. Xiong, Y. Liu, Z. Ju, Y. Qian, High electrochemical performance of monodisperse NiCo2O4 mesoporous microspheres as an anode material for Li-ion batteries, ACS applied materials & interfaces, 5 (2013) 981-988.
[42] L. Qian, L. Gu, L. Yang, H. Yuan, D. Xiao, Direct growth of NiCo 2 O 4 nanostructures on conductive substrates with enhanced electrocatalytic activity and stability for methanol oxidation, Nanoscale, 5 (2013) 7388-7396.
[43] G. Zhang, Controlled growth of NiCo2O4 nanorods and ultrathin nanosheets on carbon nanofibers for high-performance supercapacitors, Scientific reports, 3 (2013) 1-6.
[44] L. Yu, G. Zhang, C. Yuan, X.W.D. Lou, Hierarchical NiCo 2 O 4@ MnO 2 core–shell heterostructured nanowire arrays on Ni foam as high-performance supercapacitor electrodes, Chemical Communications, 49 (2013) 137-139.
[45] G.Q. Zhang, H.B. Wu, H.E. Hoster, M.B. Chan-Park, X.W.D. Lou, Single-crystalline NiCo 2 O 4 nanoneedle arrays grown on conductive substrates as binder-free electrodes for high-performance supercapacitors, Energy & Environmental Science, 5 (2012) 9453-9456.
[46] Q. He, J. Liu, X. Liu, G. Li, D. Chen, P. Deng, J. Liang, Fabrication of amine-modified magnetite-electrochemically reduced graphene oxide nanocomposite modified glassy carbon electrode for sensitive dopamine determination, Nanomaterials, 8 (2018) 194.
[47] Y. Zhou, L. Ma, M. Gan, M. Ye, X. Li, Y. Zhai, F. Yan, F. Cao, Monodisperse MnO2@ NiCo2O4 core/shell nanospheres with highly opened structures as electrode materials for good-performance supercapacitors, Applied Surface Science, 444 (2018) 1-9.
[48] E. Jokar, A.I. Zad, S. Shahrokhian, Synthesis and characterization of NiCo 2 O 4 nanorods for preparation of supercapacitor electrodes, Journal of Solid State Electrochemistry, 19 (2015) 269-274.
[49] Q. Chu, B. Yang, W. Wang, W. Tong, X. Wang, X. Liu, J. Chen, Fabrication of a Stainless-Steel-Mesh-Supported Hierarchical Fe2O3@ NiCo2O4 Core-Shell Tubular Array Anode for Lithium-Ion Battery, ChemistrySelect, 1 (2016) 5569-5573.
[50] G. Huang, L. Zhang, F. Zhang, L. Wang, Metal–organic framework derived Fe 2 O 3@ NiCo 2 O 4 porous nanocages as anode materials for Li-ion batteries, Nanoscale, 6 (2014) 5509-5515.
[51] K. Xu, X. Yang, J. Yang, J. Hu, Synthesis of hierarchical Co3O4@ NiCo2O4 core-shell nanosheets as electrode materials for supercapacitor application, Journal of Alloys and Compounds, 700 (2017) 247-251.
[52] A. Parkash, T. Ng, W. Tso, Purification and characterization of charantin, a napin-like ribosome-inactivating peptide from bitter gourd (Momordica charantia) seeds, The Journal of peptide research, 59 (2002) 197-202.
[53] G. Cousens, There is a cure for diabetes: the tree of life 21-day+ program, North Atlantic Books2007.

[54] D. Katiyar, V. Singh, M. Ali, Phytochemical and Pharmacological Profile of Momordica charantia: A Review, Biochemistry and Therapeutic Uses of Medicinal Plants, Edited by: Prof, Abbas Ali Mahdi, Prof. YK Sharma, Murtaza Abid and Dr. MM Abid Ali Khan, (2017).
[55] S. Amin, A. Tahira, A.R. Solangi, R. Mazzaro, Z.H. Ibupoto, A. Fatima, A. Vomiero, Functional nickel oxide nanostructures for ethanol oxidation in alkaline media, Electroanalysis, 32 (2020) 1052-1059.
[56] P. Chettri, V. Vendamani, A. Tripathi, M.K. Singh, A.P. Pathak, A. Tiwari, Green synthesis of silver nanoparticle-reduced graphene oxide using Psidium guajava and its application in SERS for the detection of methylene blue, Applied Surface Science, 406 (2017) 312-318.
[57] I. Saafi, R. Dridi, A. Mami, J. Ben Naceur, A. Amlouk, R. Chtourou, M. Amlouk, Some physical investigations on NiCo 2 O 4 thin films for potential applications, Applied Physics A, 127 (2021) 1-12.
[58] M. Hashem, E. Saion, N.M. Al-Hada, H.M. Kamari, A.H. Shaari, Z.A. Talib, S.B. Paiman, M.A. Kamarudeen, Fabrication and characterization of semiconductor nickel oxide (NiO) nanoparticles manufactured using a facile thermal treatment, Results in physics, 6 (2016) 1024-1030.
[59] Z.H. Ibupoto, A. Tahira, A.A. Shah, U. Aftab, M.Y. Solangi, J.A. Leghari, A.H. Samoon, A.L. Bhatti, M.A. Bhatti, R. Mazzaro, NiCo2O4 nanostructures loaded onto pencil graphite rod: An advanced composite material for oxygen evolution reaction, International Journal of Hydrogen Energy, 47 (2022) 6650-6665.
[60] B. Hu, J. Yuan, J. Zhang, Q. Shu, D. Guan, G. Yang, W. Zhou, Z. Shao, High activity and durability of a Pt–Cu–Co ternary alloy electrocatalyst and its large-scale preparation for practical proton exchange membrane fuel cells, Composites Part B: Engineering, 222 (2021) 109082.
[61] A. Hanan, M. Ahmed, M.N. Lakhan, A.H. Shar, D. Cao, A. Asif, A. Ali, M. Gul, Novel rGO@ Fe3O4 nanostructures: An active electrocatalyst for hydrogen evolution reaction in alkaline media, Journal of the Indian Chemical Society, 99 (2022) 100442.
[62] W.C. Huo, X.L. Liu, Y.S. Yuan, N. Li, T. Lan, X.Y. Liu, Y.X. Zhang, Facile synthesis of manganese cobalt oxide/nickel cobalt oxide composites for high-performance supercapacitors, Frontiers in Chemistry, 6 (2019) 661.
[63] M. Gong, W. Zhou, M.-C. Tsai, J. Zhou, M. Guan, M.-C. Lin, B. Zhang, Y. Hu, D.-Y. Wang, J. Yang, Nanoscale nickel oxide/nickel heterostructures for active hydrogen evolution electrocatalysis, Nature communications, 5 (2014) 4695.
[64] A.G. Solangi, A. Tahira, B. Waryani, A.S. Chang, T. Pirzada, A. Nafady, E.A. Dawi, L.M. Saleem, M. Padervand, A.A.K. Haj Ismail, Green-Mediated Synthesis of NiCo2O4 Nanostructures Using Radish White Peel Extract for the Sensitive and Selective Enzyme-Free Detection of Uric Acid, Biosensors, 13 (2023) 780.
[65] S. Kumar, A. Tahira, A.L. Bhatti, M.A. Bhatti, R.H. Mari, N.M. Shaikh, M.Y. Solangi, A. Nafady, M. Emo, B. Vigolo, Transforming NiCo 2 O 4 nanorods into nanoparticles using citrus lemon juice enhancing electrochemical properties for asymmetric supercapacitor and water oxidation, RSC advances, 13 (2023) 18614-18626.
[66] K.K. Naik, S. Kumar, C.S. Rout, Electrodeposited spinel NiCo 2 O 4 nanosheet arrays for glucose sensing application, RSC Advances, 5 (2015) 74585-74591.
[67] K.-b. Jang, K.R. Park, K.M. Kim, S.-k. Hyun, J.-e. Jeon, Y.S. Song, S.-k. Park, K.-i. Moon, C. Ahn, S.-c. Lim, Synthesis of NiCo2O4 nanostructures and their electrochemial properties for glucose detection, Nanomaterials, 11 (2020) 55.
[68] X. Liu, X. Zhang, Y. Liu, M. Liu, X. Miao, Y. Wang, Influence of ZnS crystal morphology on adsorption-photocatalytic efficiency of pseudocrystal ZnS nanomaterials for methylene blue degradation, Journal of Molecular Structure, 1256 (2022) 132514.
[69] Y. Zhang, H. Liu, L. Ning, W. Gu, X. Liu, A novel core-shell upconversion nanoparticles@ zirconium-based metal organic framework fluorescent nanoprobe for efficient continuous detection of trace methylene blue and ferrous ions, Talanta, 224 (2021) 121853.

[70] N. Bélaz-David, L. Decosterd, M. Appenzeller, Y. Ruetsch, R. Chioléro, T. Buclin, J. Biollaz, Spectrophotometric determination of methylene blue in biological fluids after ion-pair extraction and evidence of its adsorption on plastic polymers, European journal of pharmaceutical sciences, 5 (1997) 335-345.
[71] R.S. Razmara, A. Daneshfar, R. Sahrai, Determination of methylene blue and sunset yellow in wastewater and food samples using salting-out assisted liquid–liquid extraction, Journal of Industrial and Engineering Chemistry, 17 (2011) 533-536.
[72] P. Arias, N.F. Ferreyra, G.A. Rivas, S. Bollo, Glassy carbon electrodes modified with CNT dispersed in chitosan: analytical applications for sensing DNA–methylene blue interaction, Journal of Electroanalytical Chemistry, 634 (2009) 123-126.
[73] M.L. Wen, Y.B. Zhao, X. Chen, C.Y. Wang, Potentiometric sensor for methylene blue based on methylene blue–silicotungstate ion association and its pharmaceutical applications, Journal of pharmaceutical and biomedical analysis, 18 (1999) 957-961.
[74] I.K. Tonlé, E. Ngameni, H.L. Tcheumi, V. Tchiéda, C. Carteret, A. Walcarius, Sorption of methylene blue on an organoclay bearing thiol groups and application to electrochemical sensing of the dye, Talanta, 74 (2008) 489-497.
[75] S. Sangeetha, G. Krishnamurthy, M.S. Raghavan, Electrochemical sensing and photocatalytic degradation of methylene blue (MB) dye by cobalt-beta hydroxy benzoate complex, Materials Science in Semiconductor Processing, 101 (2019) 164-173.
[76] M. Rani, U. Shanker, Efficient degradation of organic pollutants by novel titanium dioxide coupled bismuth oxide nanocomposite: Green synthesis, kinetics and photoactivity, Journal of Environmental Management, 300 (2021) 113777.
[77] M. Aravind, M. Amalanathan, M.S.M. Mary, Synthesis of TiO 2 nanoparticles by chemical and green synthesis methods and their multifaceted properties, SN Applied Sciences, 3 (2021) 1-10.
[78] N. Gavade, K. Garadkar, GV Khade, MB Suwarnkar, J Mater Sci: Mater Electron, 26 (2015) 3309-3315.
[79] S. Alkaykh, A. Mbarek, E.E. Ali-Shattle, Photocatalytic degradation of methylene blue dye in aqueous solution by MnTiO3 nanoparticles under sunlight irradiation, Heliyon, 6 (2020).
[80] Z. Vasiljevic, M. Dojcinovic, J. Vujancevic, I. Jankovic-Castvan, M. Ognjanovic, N. Tadic, S. Stojadinovic, G. Brankovic, M. Nikolic, Photocatalytic degradation of methylene blue under natural sunlight using iron titanate nanoparticles prepared by a modified sol–gel method, Royal Society open science, 7 (2020) 200708.
[81] M.A. Bhatti, K.F. Almaani, A.A. Shah, A. Tahira, A.D. Chandio, A.Q. Mugheri, A.l. Bhatti, B. Waryani, S.S. Medany, A. Nafady, Low temperature aqueous chemical growth method for the doping of W into ZnO nanostructures and their photocatalytic role in the degradration of methylene blue, Journal of Cluster Science, (2022) 1-12.
[82] M.A. Bhatti, S.J. Gilani, A.A. Shah, I.A. Channa, K.F. Almani, A.D. Chandio, I.A. Halepoto, A. Tahira, M.N. Bin Jumah, Z.H. Ibupoto, Effective removal of methylene blue by surface alteration of TiO2 with Ficus Carica leaf extract under visible light, Nanomaterials, 12 (2022) 2766.

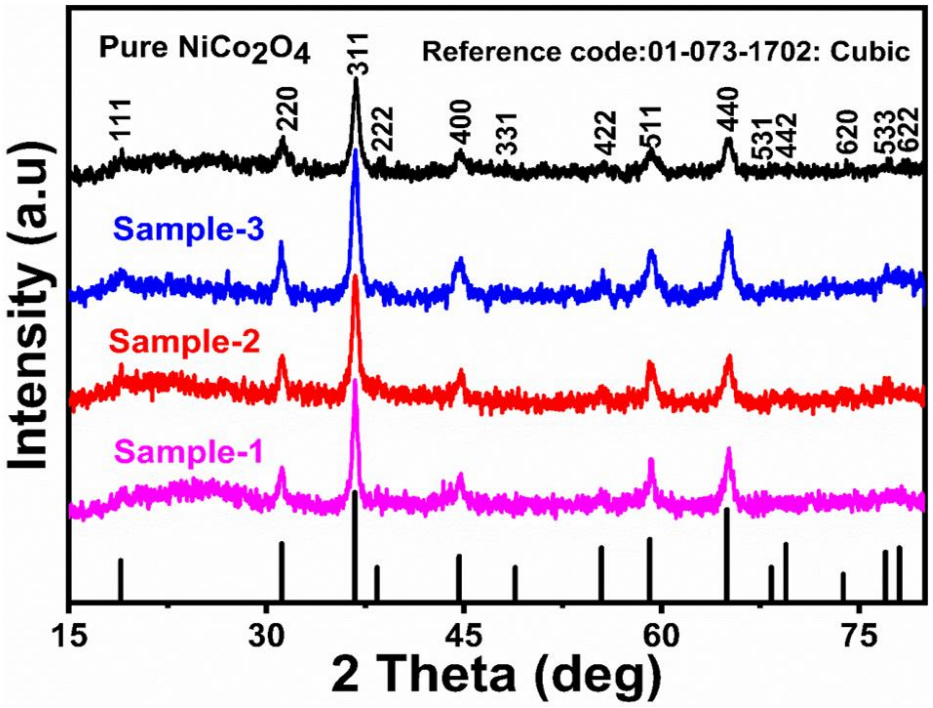
Pure NiCo2O4
Reference code:01-073-1702: Cubic
111
220
311
222
400
331
422
511
440
531
442
620
533
622
Sample-3
Sample-2
Sample-1
Intensity (a.u)
15
30
45
60
75
2 Theta (deg)

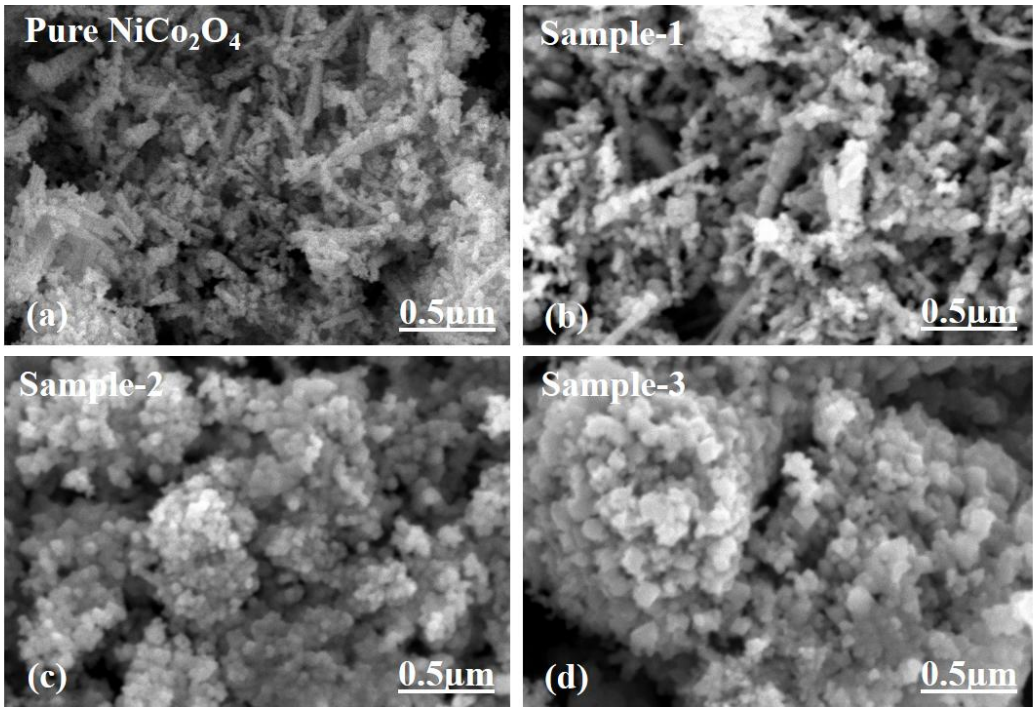
Pure $NiCo_2O_4$
(a)
0.5µm
Sample-1
(b)
0.5µm
Sample-2
(c)
0.5µm
Sample-3
(d)
0.5µm

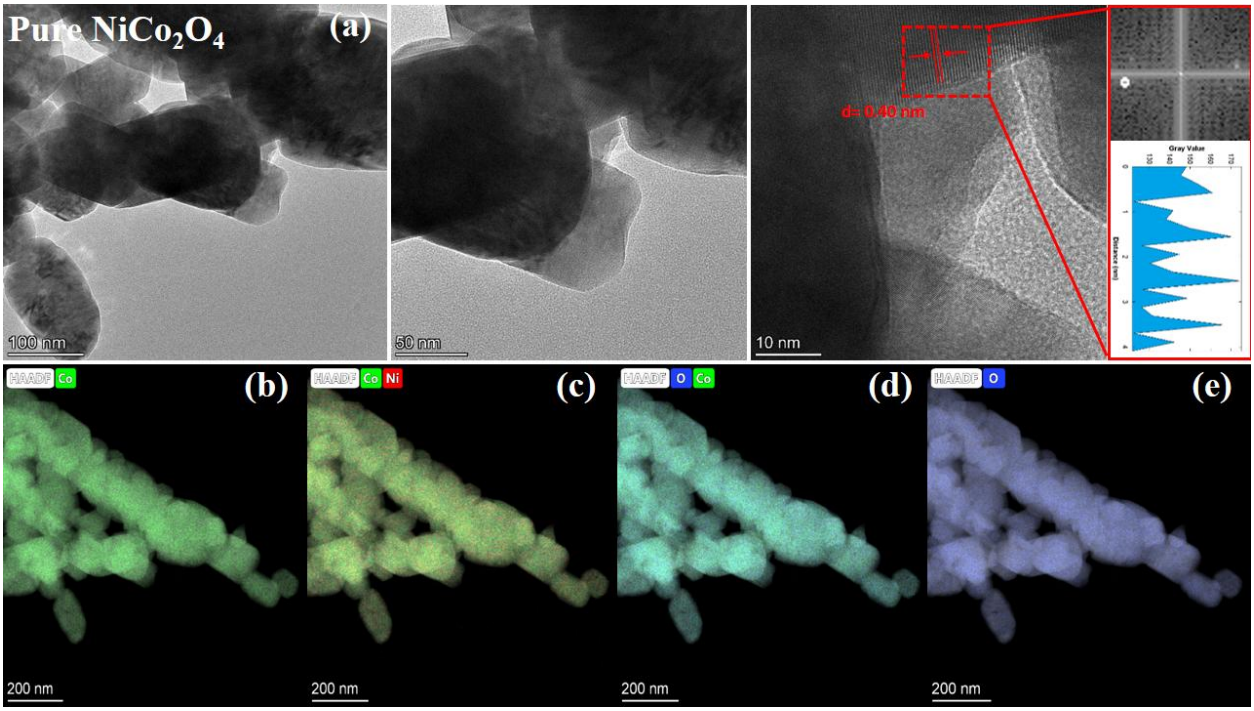
Pure $NiCo_2O_4$
(a)
100 nm
50 nm
d= 0.40 nm
10 nm
Gray Value
Distance (nm)
HAADF Co
(b)
200 nm
HAADF Co Ni
(c)
200 nm
HAADF O Co
(d)
200 nm
HAADF O
(e)
200 nm

Fig. 1 (a) Pristine material and its corresponding d-spacing value along with FFT transformation (b), (c), (d), and (d) Elemental mapping of desired material

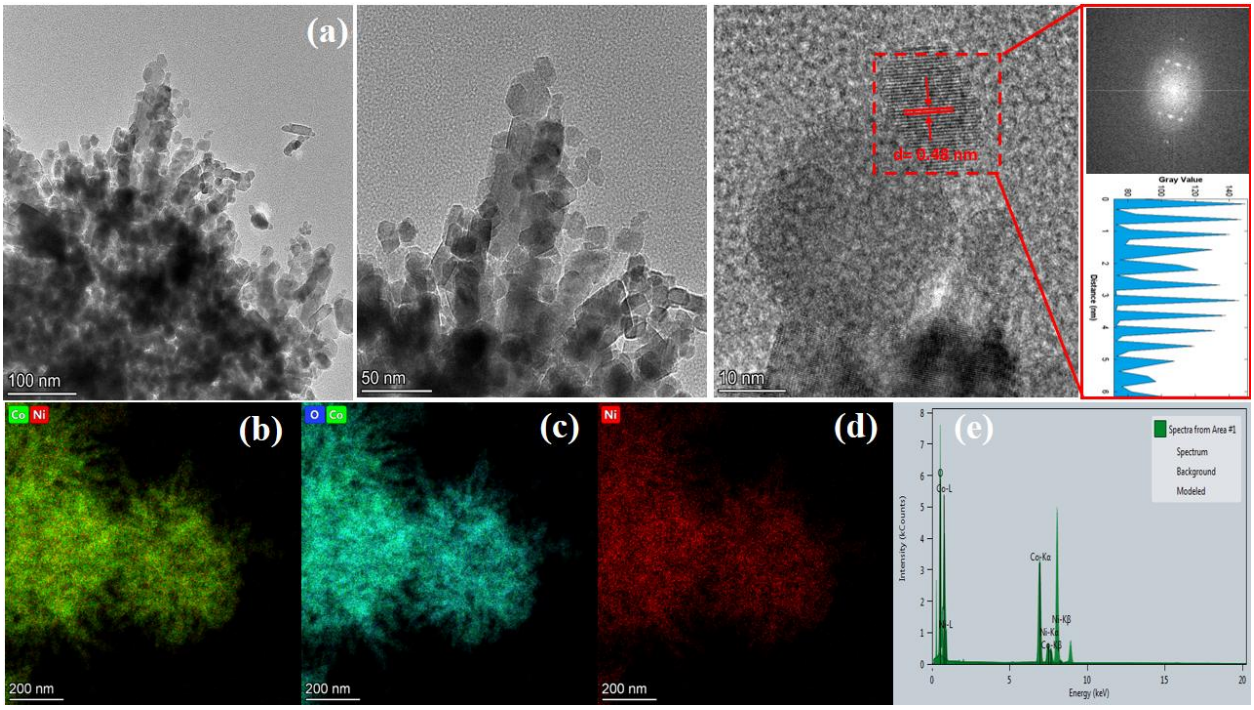

Fig. 2 (a) Targeted Material and its corresponding d-spacing value along with FFT transformation (b), (c), (d), and (d) Elemental mapping of desired material (e) EDS spectra for elemental composition

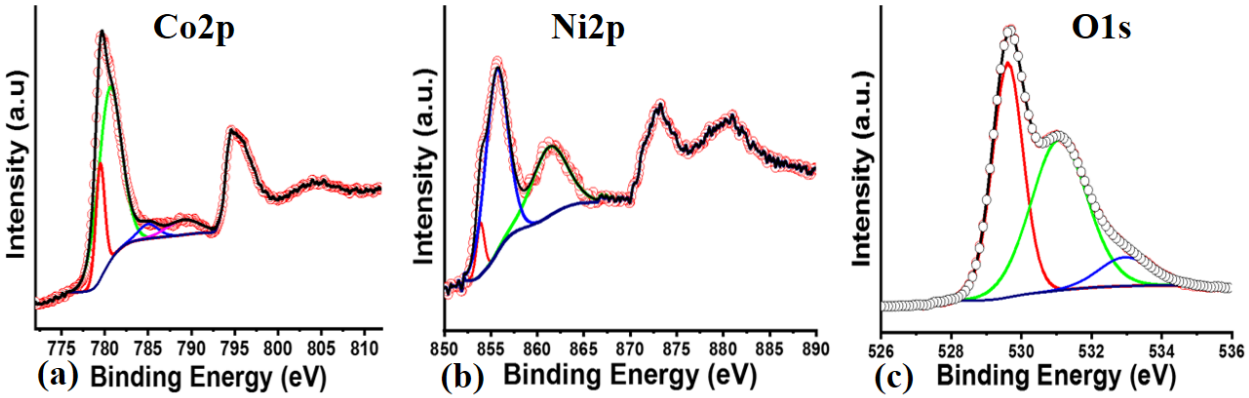

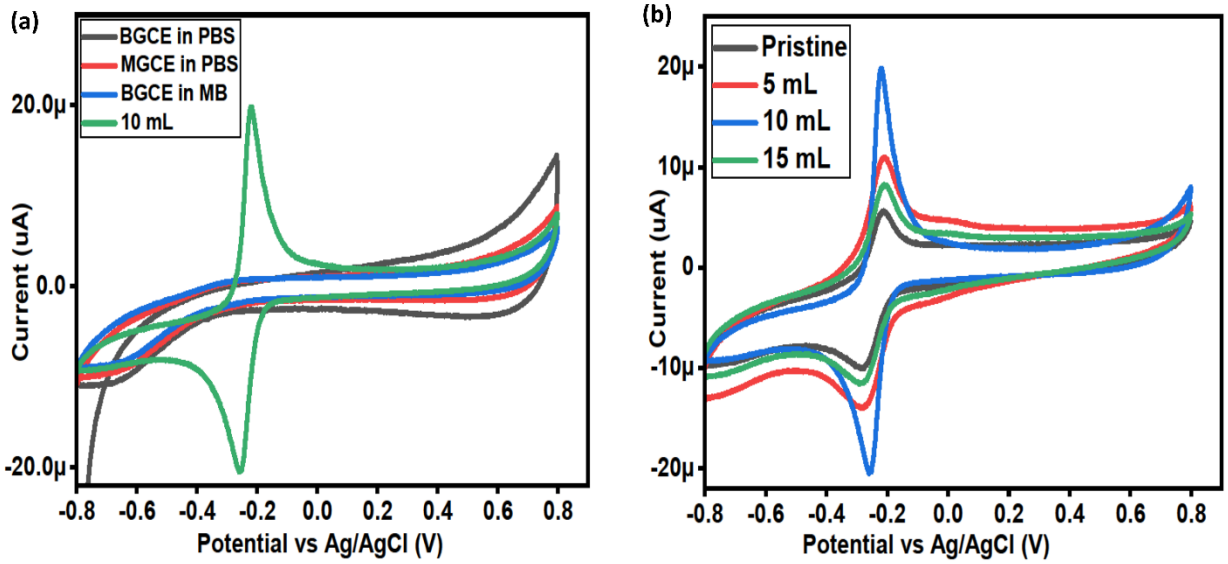

Fig. (a) Cyclic voltammogram of bare GCE in electrolyte and in the presence of MB, and of GCE modified with 5 mL in the presence of 0.5 mM MB in 0.1M PBS at a scan rate of 50 mV/s. **(b)** Cyclic voltammograms of MGCE of 5 mL, 10 mL, 15 mL and pristine $NiCo_2O_4$-modified GCE in the presence of 0.5 mM of MB in 0.1M PBS at a scan rate of 50 mV/s,

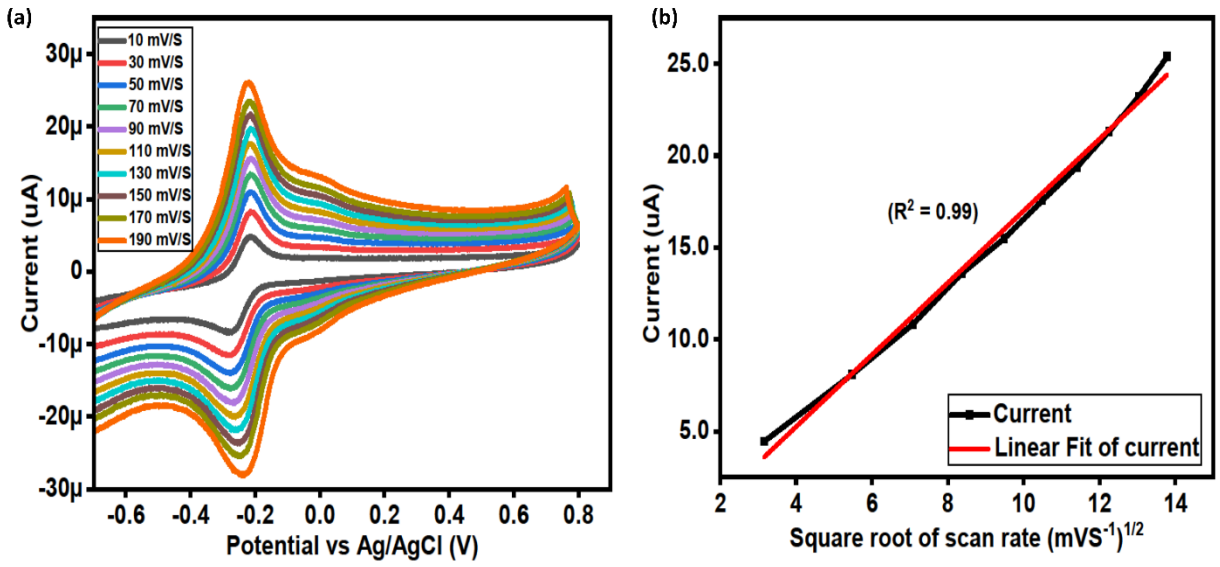

Fig. (a) Cyclic voltammograms of 10 mL collected in 0.5 mM MB solution in 0.1M PBS at different scan rates; **(b)** sensor anodic current as a function of the square root of scan rate.

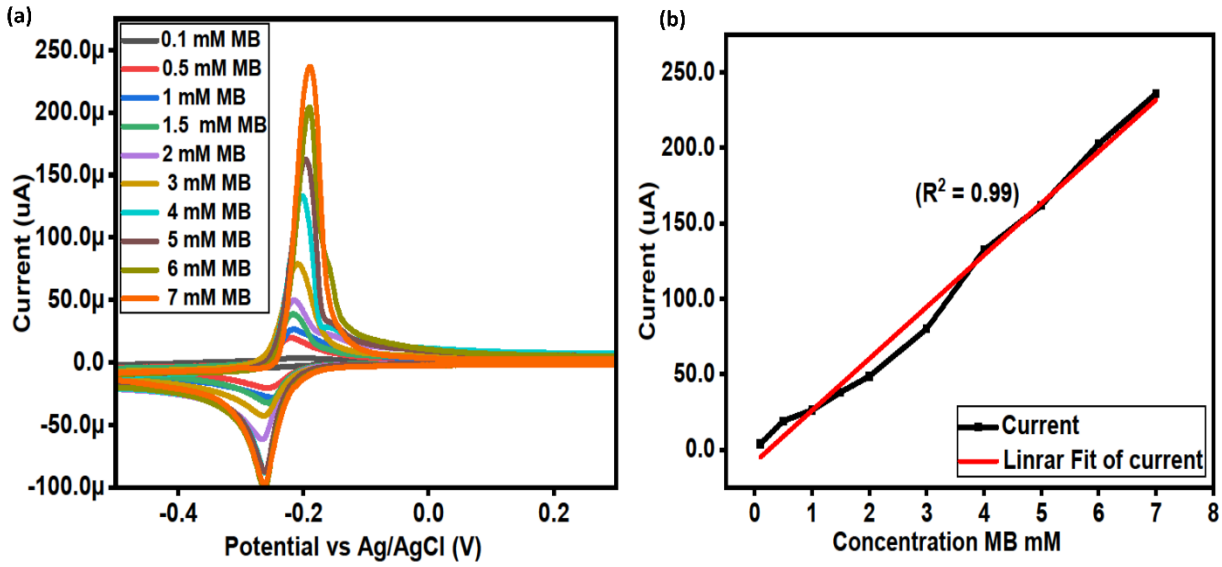

Fig. 5 (a) Cyclic voltammograms for 10 mL at different MB concentrations in 0.1M PBS at a scan rate of 50 mV/s, **(b)** sensor anodic current as a function of MB concentration.

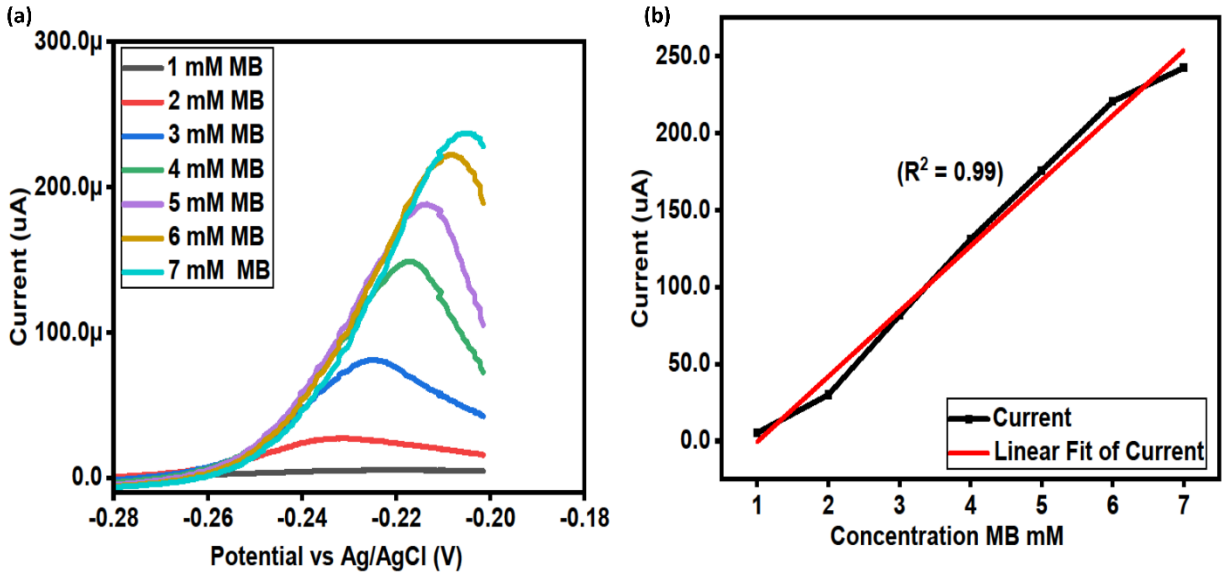

Fig. (a) Linear sweep voltammogram for 5 mL at different MB concentrations in 0.1M PBS **(b)** sensor anodic current as a function of MB concentration.

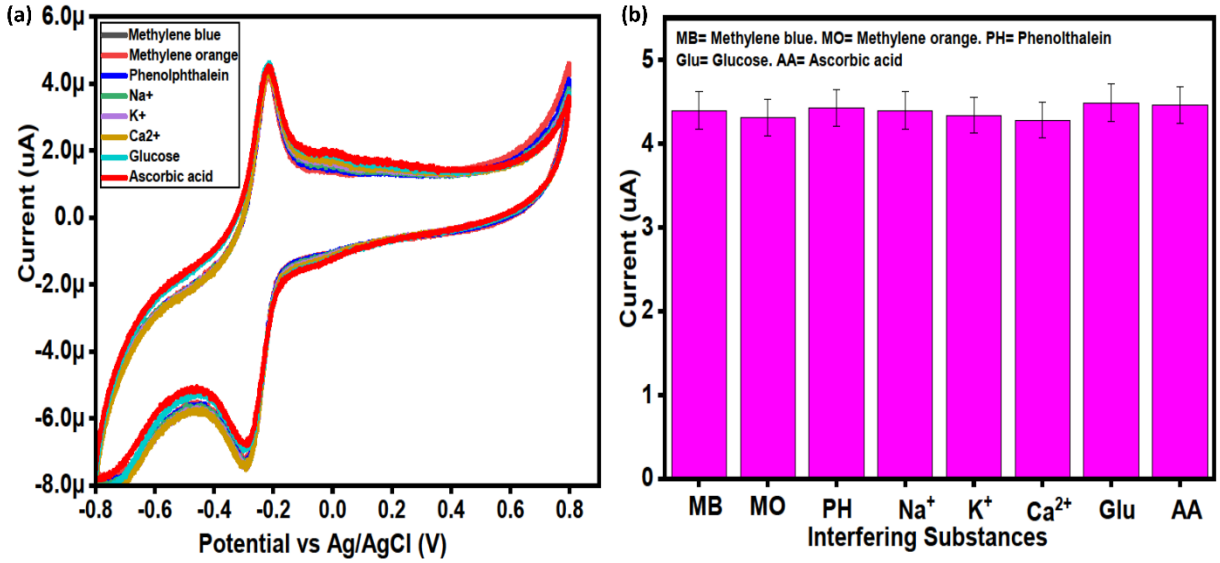

Fig. (a) Cyclic voltammograms of 10 mL collected in presence of 0.1 mM solutions of MB in 0.1M, several potential interferers at a scan rate of 50 mV/s. **(b)** Bar graph of various interfering substances. Stability study of 10 mL collecting 20 cycles in presence of 0.5 mM MB in 0.1M PBS at a scan rate of 50 mV/s.

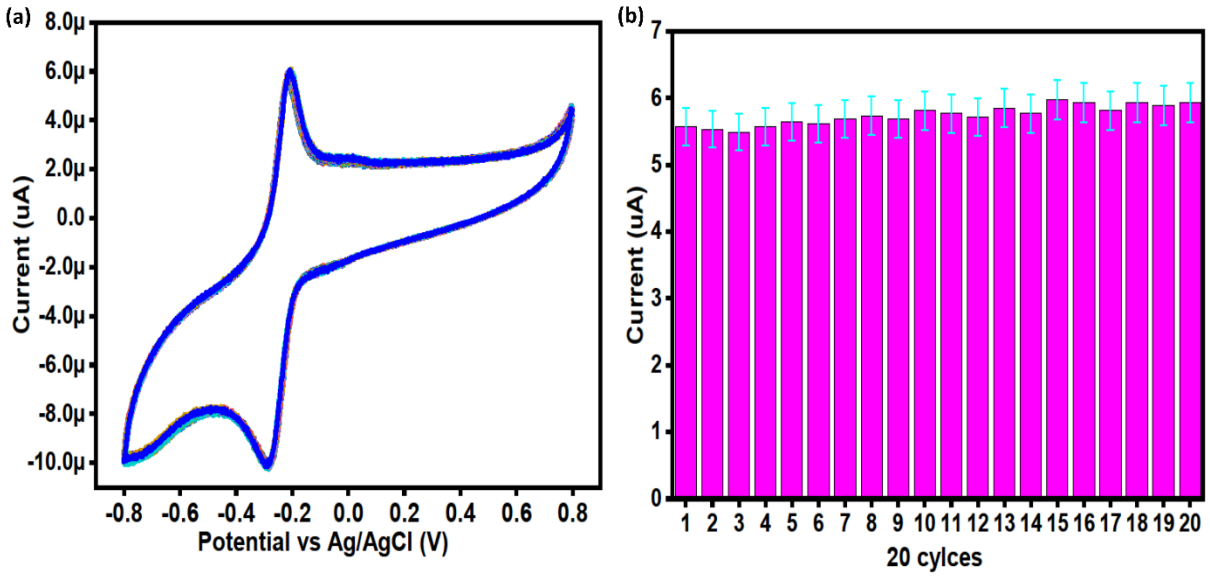

Fig. **(a)** Stability study of 10 mL collecting 20 cycles in presence of 0.1 mM MB in 0.1M PBS at a scan rate of 50 mV/s. **(b)** Bar graph of 20 cycles.

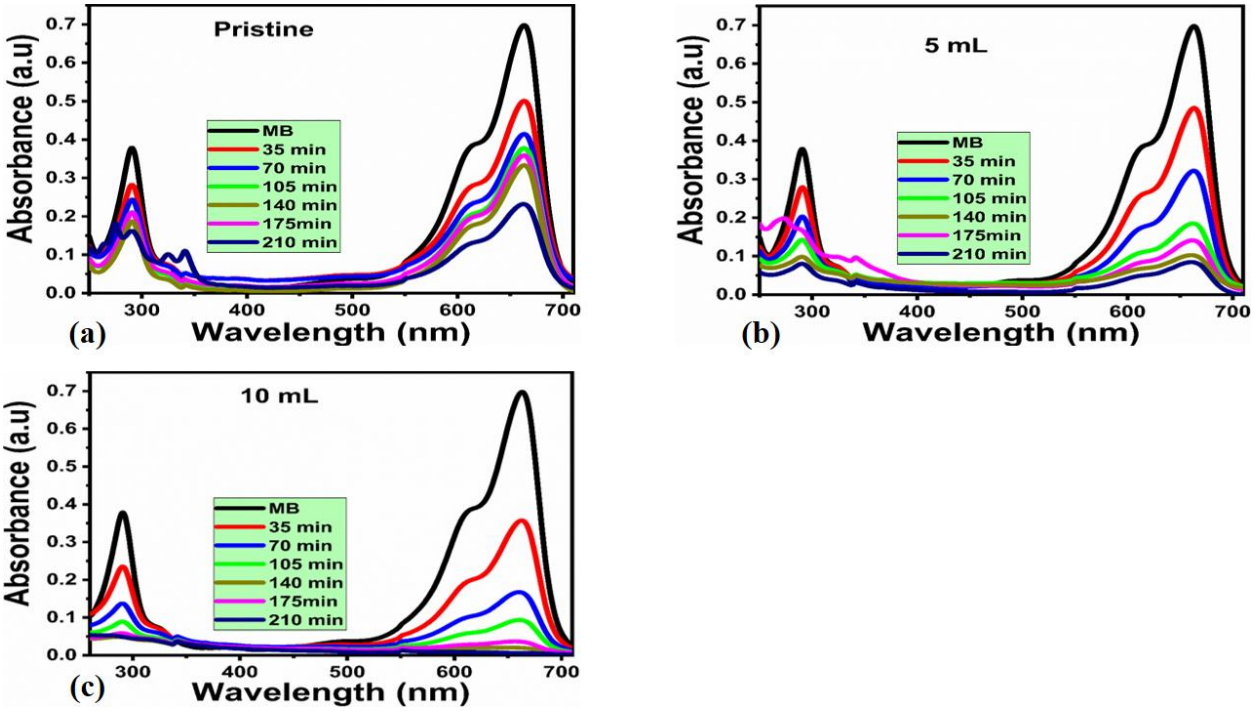

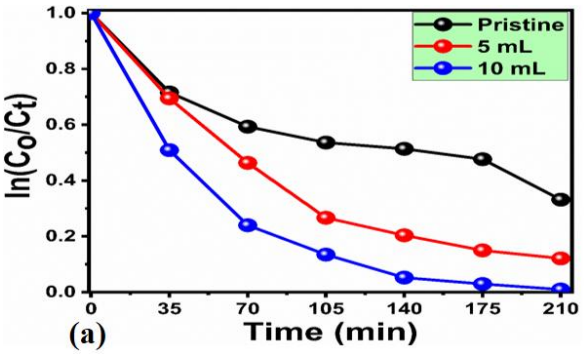
Pristine
5 mL
10 mL
ln(C0/Ct)
Time (min)
(a)

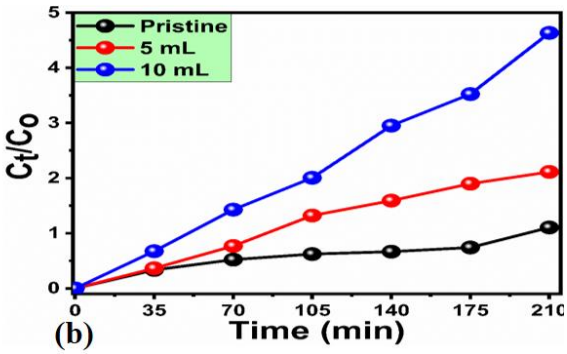
Pristine
5 mL
10 mL
Ct/C0
Time (min)
(b)

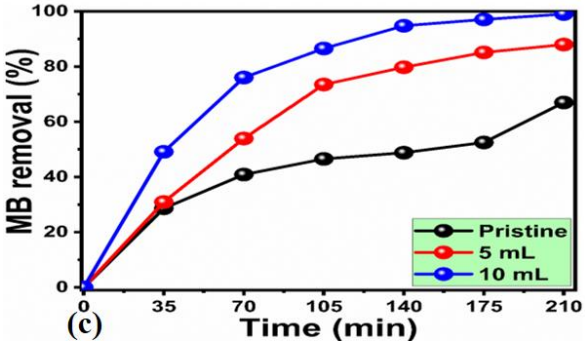
Pristine
5 mL
10 mL
MB removal (%)
Time (min)
(c)